High entropy design endows spinel compounds with excellent bifunctional catalysis for hydrogen production from water electrolysis

Mingxu Li, Xiaolei Ye, Shenghui Guo, Ming Hou, Li Yang, Kaihua Chen, Lei Gao, Yunchuan Li, Pascal Briois

▶ **To cite this version:**

Mingxu Li, Xiaolei Ye, Shenghui Guo, Ming Hou, Li Yang, et al.. High entropy design endows spinel compounds with excellent bifunctional catalysis for hydrogen production from water electrolysis. International Journal of Hydrogen Energy, 2025, 130, pp.644-653. ⟨10.1016/j.ijhydene.2025.04.364⟩. ⟨hal-05529523⟩

HAL Id: hal-05529523

https://hal.science/hal-05529523v1

Submitted on 27 Feb 2026

HAL is a multi-disciplinary open access archive for the deposit and dissemination of scientific research documents, whether they are published or not. The documents may come from teaching and research institutions in France or abroad, or from public or private research centers.

L'archive ouverte pluridisciplinaire **HAL**, est destinée au dépôt et à la diffusion de documents scientifiques de niveau recherche, publiés ou non, émanant des établissements d'enseignement et de recherche français ou étrangers, des laboratoires publics ou privés.

HAL Authorization

High entropy design endows spinel compounds with excellent bifunctional catalysis for hydrogen production from water electrolysis

Mingxu LI [1, 2, 3], Xiaolei YE [1, 2, 3*], Shenghui GUO [1, 2, 3], Ming HOU [1, 2, 3], Li YANG [1, 2, 3*], Kaihua CHEN[1, 3], Lei GAO [1, 2, 3], Yunchuan LI [1, 3], Pascal BRIOIS[4]

1. Faculty of Metallurgical and Energy Engineering, Kunming University of Science and Technology, Kunming 650093, China
2. State International Joint Research Center of Advanced Technology for Superhard Materials, Kunming University of Science and Technology, Kunming 650093, China
3. State Key Laboratory of Complex Nonferrous Metal Resources Clean Utilization; Faculty of Metallurgical and Energy Engineering, Kunming University of Science and Technology, Kunming 650093, China
4. FEMTO-ST Institute (UMR CNRS 6174), UBFC/UTBM. Site de Montbéliard, F-90010 Belfort-France

Corresponding author:

Xiaolei YE (Stoneye2@163.com)

Li YANG (yanglikmust@163.com)

Abstracts： Promoting the use of hydrogen energy is considered an effective strategy to address current energy and environmental challenges. Developing efficient and cost-effective bifunctional catalysts is crucial for advancing hydrogen production. In this study, novel high-entropy spinel oxide $(FeCoNiCrZnCu)_3O_4$ was successfully synthesized via a microwave hydrothermal method as a catalyst for water electrolysis under alkaline conditions. The results demonstrate that the high-entropy strategy is an effective approach to enhancing the oxygen vacancy content in spinel oxides. Additionally, compared to non-high-entropy materials, exhibited an increased specific surface area, indicating that the high-entropy strategy also positively impacts the surface morphology. Benefiting from the increased oxygen vacancy content and the synergistic effect of multi-metal cations, $(FeCoNiCrZnCu)_3O_4$ showed exceptional bifunctional catalytic performance in water electrolysis. At a current density of 10 mA cm^{-2}, the corrected hydrogen evolution overpotential and oxygen evolution overpotential were only 133 mV and 357 mV, respectively. This work provides valuable insights into the application of high-entropy spinel materials in hydrogen production via water electrolysis.

Keywords: High entropy spinel, microwave synthesis, bifunctional catalysis, oxygen vacancies, water electrolysis

1 Introduction

Since the Industrial Revolution, fossil energy, with their stability and high reliability, have been instrumental in driving the development of human society and economic growth [1-4]. However, human society is facing a major crisis triggered by the overconsumption of fossil fuels, which includes the increasing depletion of resources and the exacerbation of environmental pollution [5-7]. Developing renewable and clean energy is essential for ensuring the sustainable development of human society [8]. Hydrogen energy, especially green hydrogen energy, is widely regarded as one of the most promising clean energy sources due to its excellent high energy density and environmentally friendly characteristics [9]. Hydrogen production through water electrolysis is considered a promising strategy for reducing fossil fuel consumption and

promoting sustainable energy [10]. However, efficient catalysts are crucial in the water electrolysis process to overcome the reaction energy barriers associated with this non-spontaneous reaction [11].

Conventional noble metal-based electrocatalysts (Pt-group metals, Ru/Ir oxides) demonstrate exceptional electrocatalytic activity in both the hydrogen evolution reaction (HER) and oxygen evolution reaction (OER) are currently being commercialized for water electrolysis [12]. Nevertheless, the high cost of Pt and RuO_2 limits their large-scale commercial application. Currently, relatively inexpensive transition metal-based catalysts, including hydroxides [13], oxides [14, 15] , phosphides [16], sulfides [17], and nitrides [18] are are being explored as viable alternatives for water electrolysis. A well-established hierarchy of oxidative resilience emerges in transition metal compounds: sulfides demonstrate compromised phase stability relative to oxides under equivalent oxidizing conditions, while nitrides and phosphides undergo accelerated degradation kinetics surpassing even sulfide counterparts [19-21].

During the development of materials, man has improved or developed new materials by mixing together materials with different properties. Inspired by this, in 2015, Rost et al [22] extended the high entropy strategy to the field of oxides and synthesized the (CoCuMgNiZn)O single-phase solid solution for the first time. They confirmed the positive role of high mixing entropy in phase stabilization and proposed a new material system, namely high-entropy oxides (HEOs). In recent years, high entropy spinel oxides (HESO) have garnered interest in the domains of energy storage and catalysis because of their intriguing characteristics for Li^+ storage [23]. However, there are limited reports on the application of HESO as catalysts in water electrolysis, with only a few studies highlighting their high efficiency in the OER process. Sun et al.[24] found that compared with $(FeMnNi)_3O_4$, equimolar $(Cr_{0.2}Mn_{0.2}Fe_{0.2}Co_{0.2}Ni_{0.2})_3O_4$ (CMFCN) can achieve efficient OER process with lower overpotential (322 mV) in KOH alkaline solution and maintain higher stability. The CMFCN synthesized by He et al. exhibits an increased grain boundary density, which significantly enhances the kinetics of the OER. As a result, the OER overpotential in KOH alkaline solution is reduced to 275 mV [25]. The central motivation for the preparation of high-entropy

oxide materials, such as $(FeCoNiCrZnCu)_3O_4$, stems from the significant shortcomings of conventional oxide materials and their performance bottlenecks in electrolytic water-to-hydrogen applications, and the unique design of high-entropy materials that can break through these limitations. HER remains a primary bottleneck constraining the energy efficiency of water electrolysis for hydrogen generation. High-entropy oxide systems (HESO) exhibit exceptional adaptability in modulating their elemental configurations and charge distribution characteristics. Therefore, designing HESO through a high-entropy strategy to achieve bifunctional catalysis for both HER and OER is crucial for maximizing their potential in water electrolysis applications.

In this work, $(FeCoNiCrZnCu)_3O_4$ catalysts were synthesized using the microwave hydrothermal method, which provides an efficient and time-saving approach for precisely controlling the composition, structure, and morphology of the materials. The microscopic morphology of the catalyst was thoroughly characterized using transmission electron microscopy (TEM) and scanning electron microscopy (SEM). The influence of different elemental compositions on the catalytic performance, including both the oxygen OER and HER, was investigated. Additionally, the specific surface area and oxygen vacancy content of the catalysts were analyzed using a fully automated specific surface and porosity analyzer (BET) and an electron spin resonance spectrometer (ESR/EPR). A comprehensive comparison of the microstructure and properties of $(FeCoNiCrZnCu)_3O_4$ versus traditional non-high-entropy spinels was also conducted. The bifunctional catalytic performance of the $(FeCoNiCrZnCu)_3O_4$ synthesized in this work offers valuable insights for the development of advanced catalysts for water electrolysis.

2 Experimental

2.1 Materials

Cobalt nitrate hydrate ($Co(NO_3)_3 \cdot 6H_2O$), iron nitrate hydrate ($Fe(NO_3)_3 \cdot 9H_2O$), nickel nitrate hydrate ($Ni(NO_3)_2 \cdot 6H_2O$), chromium nitrate hydrate ($Cr(NO_3)_3 \cdot 9H_2O$), zinc nitrate hydrate ($Zn(NO_3)_2 \cdot 6H_2O$), copper nitrate trihydrate ($Cu(NO_3)_2 \cdot 3H_2O$), urea ($CO(NH_2)_2$) were purchased from Aladdin Reagent Co. Potassium hydroxide (KOH) and anhydrous ethanol (CH_3CH_2OH) were purchased from Tianjin Zhiyuan

Chemical Reagent Co. Acetone and hydrochloric acid were purchased from Chuandong Chemical Co.

2.2 Material synthesis

High-entropy oxides were synthesized from metal nitrates as starting materials as show in **Fig.1**. To begin, 0.001 mol of each metal nitrate was dissolved in water. After complete dissolution of the starting materials, urea was added as a precipitant. The resulting solution was transferred to a 500 mL polytetrafluoroethylene-lined microwave synthesis reactor. The reaction was carried out under hydrothermal conditions at 100°C for 1 hours. The formed precipitate was then washed with ethanol and deionized water, followed by centrifugation at 8000 rpm for 2 minutes. The product was dried at 80°C for 8 hours. Finally, the dried sample was annealed at 900°C in air for 2 hours to obtain the final product $(FeCoNiCrZnCu)_3O_4$.

On the conditions for the synthesis of binary spinel：To begin, 0.001 mol of each metal nitrate was dissolved in water. After complete dissolution of the starting materials, urea was added as a precipitant. The resulting solution was transferred to a 500 mL polytetrafluoroethylene-lined microwave synthesis reactor. The reaction was carried out under hydrothermal conditions at 100℃ for 1 hours. The formed precipitate was then washed with ethanol and deionized water, followed by centrifugation at 8000 rpm for 2 minutes. The product was dried at 80℃ for 8 hours to obtain the final product ($CuFe_2O_4$, $NiFe_2O_4$, $CoFe_2O_4$).

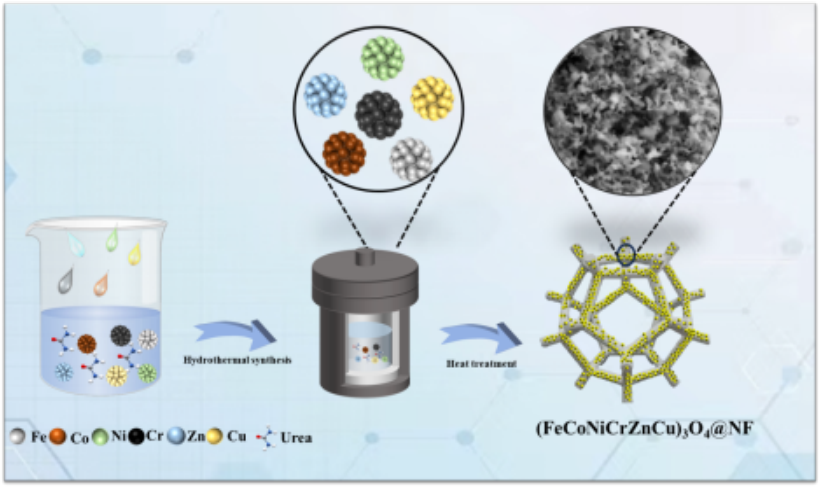

Fig.1 Syntheses of $CuFe_2O_4$, $NiFe_2O_4$, $CoFe_2O_4$, $(FeCoNiCrZnCu)_3O_4$

2.3 Electrode preparation

A mixture of 6 milligrams of the catalyst and 0.6 milligrams of carbon black was suspended in a blend of water and isopropanol (volume ratio of 10 mL:10 mL), followed by the addition of 40 μL of Nafion. The mixture was then applied to a 1.0 × 2.0 cm^2 Nickel-foam (NF) substrate. Prior to coating, the nickel foam was cleaned sequentially with acetone, aqueous hydrochloric acid (HCl: H_2O = 1:4), deionized water, and ethanol, with each solvent used for 15 minutes.

2.4 Material characterization

The phase of the high-entropy oxide was characterized using an X-ray diffraction (XRD) instrument (Rigaku Ultima IV, Japan). The high-entropy oxide's surface structure was investigated using a field-emission scanning electron microscope (FE-SEM, ZEISS GeminiSEM 300, Germany) and a transmission electron microscope (TEM, JEOL JXA-IHP200F, Japan). The specific surface area and adsorption/desorption isotherms of the high-entropy oxide were measured using a specific surface area analyzer (BET, asp-2020 plus, USA). The chemical states of the elements in the high-entropy oxide were analyzed using X-ray photoelectron spectroscopy (XPS, Thermo Scientific K-Alpha, USA). The electron spin resonance spectrometer (ESR/EPR, Bruker EMXplus-6/1, Germany) was employed to investigate substances containing unpaired electrons.

2.5 Electrochemical measurements

For the water electrolysis experiment, a series of electrochemical tests were conducted, including cyclic voltammetry (CV), linear sweep voltammetry (LSV), and electrochemical impedance spectroscopy (EIS). All tests were performed using a three-electrode system on a CS350M Electrochemical Workstation. In this setup, the NF-based composite electrode served as the working electrode, with an electrode area of 10 × 20 mm^2, and the immersed area in the solution was 10 × 10 mm^2. A saturated calomel electrode or an Ag/AgCl electrode was used as the reference electrode, while a carbon rod was employed as the counter electrode.

3 Results and discussion

X-ray diffraction (XRD) is a highly effective technique for identifying the phases of materials. The four synthesized powders were analyzed by XRD, and the results

showed that $CuFe_2O_4$, $NiFe_2O_4$, and $CoFe_2O_4$ each exhibited a single-phase spinel structure (**Fig. 2**). The main diffraction peaks for these compounds appeared at 18.453°, 30.357°, 35.760°, 37.408°, 43.466°, 53.938°, 57.503°, and 63.156°, corresponding to the crystal planes (111), (220), (311), (222), (400), (422), (511), and (440), respectively. For the $(FeCoNiCrZnCu)_3O_4$ sample, in addition to the main spinel peaks, XRD also revealed the trace amounts of CuO. The segregation of copper oxide is due to the fact that the lattice distortion of high entropy materials reduces the diffusion rate of the elements, and the copper elements may be enriched at grain boundaries or surface regions due to diffusion obstruction and react with oxygen to form CuO at high temperatures [26, 27]. A similar phenomenon has been reported in the high-entropy MAX phase material Ti-V-Cr-Mo system, in which Mo forms the sublimation phase MoO_3 due to diffusion limitation [28]. Furthermore, the microstructural information of $(FeCoNiCrZnCu)_3O_4$ was obtained by TEM characterization. According to **Fig. 3a**, the particle size distribution of this $(FeCoNiCrZnCu)_3O_4$ nanoparticles was highly consistent with the scanning electron microscopy (SEM) observations (**Fig.4**), indicating that the material was characterized by a uniform size morphology. In the high-resolution transmission electron microscopy (HRTEM) image, lattice fringes with a lattice spacing of 0.198 nm can be observed, which corresponds to the (311) crystal plane of the spinel structure (**Fig.3b**). This corresponds to the successful synthesis of high-entropy spinel phase in $(FeCoNiCrZnCu)_3O_4$ as shown by XRD. As shown in the selected area electron diffraction (SAED) analysis in **Fig.3c**, the sample presents a typical polycrystalline diffraction ring structure, and each diffraction ring corresponds to the $(FeCoNiCrZnCu)_3O_4$ crystal planes of (440), (511), (422), (400), (311), (220), and (111). These results were in good agreement with the XRD analysis [27].

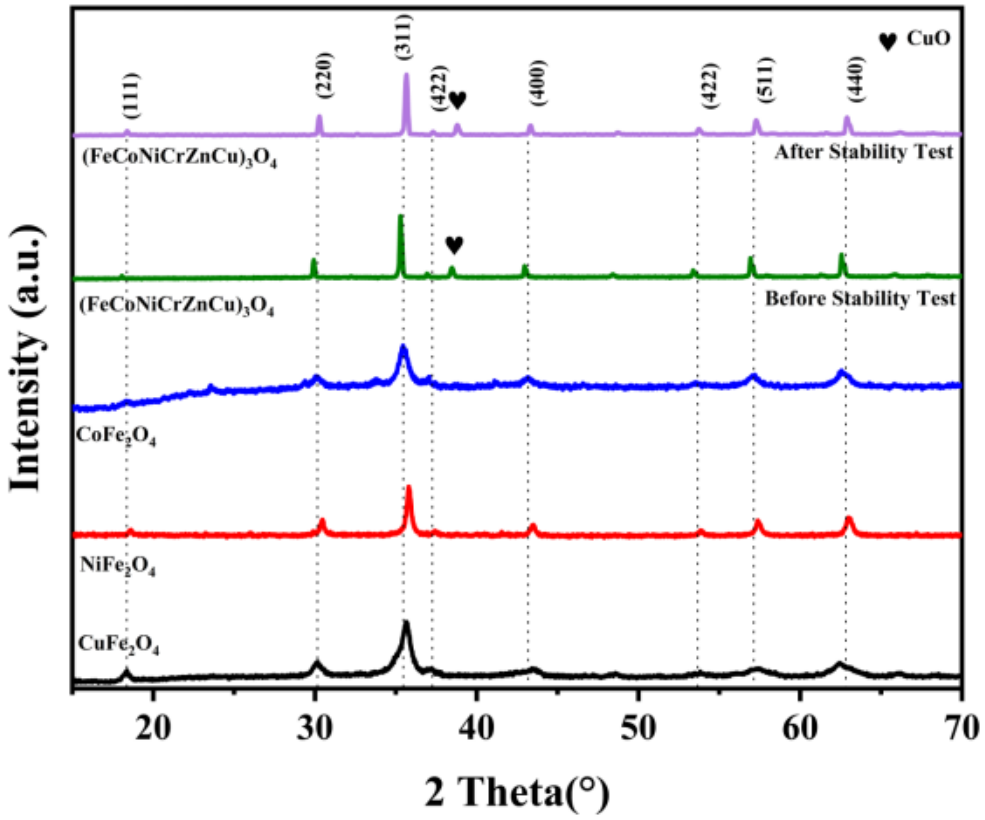

Fig.2 XRD maps of $CuFe_2O_4$, $NiFe_2O_4$, $CoFe_2O_4$, $(FeCoNiCrZnCu)_3O_4$

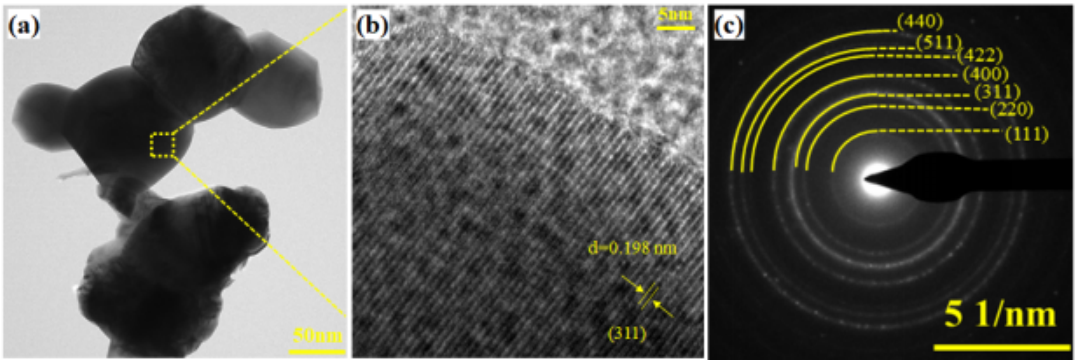

Fig.3 $(FeCoNiCrZnCu)_3O_4$ of (a)TEM image; (b) HRTEM image; (c) SAED pattern

The material's surface texture has a direct impact on the adsorption of substances within the electrolysis of water. **Fig.4** shows that the surfaces of the four materials have porous characteristics, but the differences were obvious. The surface of $(FeCoNiCrZnCu)_3O_4$ presents a rich porous structure formed by the interconnection of irregular particles. EDS mapping of the $(FeCoNiCrZnCu)_3O_4$ surface confirmed the presence of various metal elements (**Fig.5**), providing further evidence for the successful synthesis of the high-entropy spinel phase confirmed by XRD and TEM. However, EDS analysis revealed that the synthesized $(FeCoNiCrZnCu)_3O_4$ contained lower concentrations of Ni and Co, which can be attributed to the hydrothermal

synthesis process. The microwave hydrothermal method is characterized by a short reaction time (typically a few minutes) and a rapid crystallization rate. In high-entropy oxides, the entropy stabilization effect and element diffusion hysteresis may restrict the diffusion of Ni and Co, preventing them from fully incorporating into the lattice within the limited reaction time. Consequently, the Ni and Co contents in the final synthesized material were relatively low, aligning with findings from previous studies[29-31] .

The surface morphology of $CuFe_2O_4$ and $NiFe_2O_4$ was similar to flocculent precipitation with smaller pore diameters. $CoFe_2O_4$ has a porous morphology consisting of round particles with smooth surfaces and relatively large pore diameters. In order to gain a more intuitive understanding of the particular surface area and aperture dimensions of the four compounds created, N_2 adsorption-desorption tests were carried out. The specific surface area and pore size data of the synthesized materials were listed in **Fig.6**, where the specific surface areas of $(FeCoNiCrZnCu)_3O_4$, $NiFe_2O_4$, $CoFe_2O_4$, and $CuFe_2O_4$ were 26.6042 m^2/g, 19.9670 m^2/g, 16.4258 m^2/g, and 10.4041 m^2/g, respectively, while the pore sizes were centrally distributed at 43.9793 nm, 35.5442 nm, 28.4223 nm, 11.3358 nm. The specific surface area of $(FeCoNiCrZnCu)_3O_4$ was significantly larger than that of the other three materials. The smaller specific surface area of $NiFe_2O_4$ and $CuFe_2O_4$ may be due to the small pore diameter. The high specific surface area allows for the comprehensive exposure of active sites and promote the HER and OER processes.

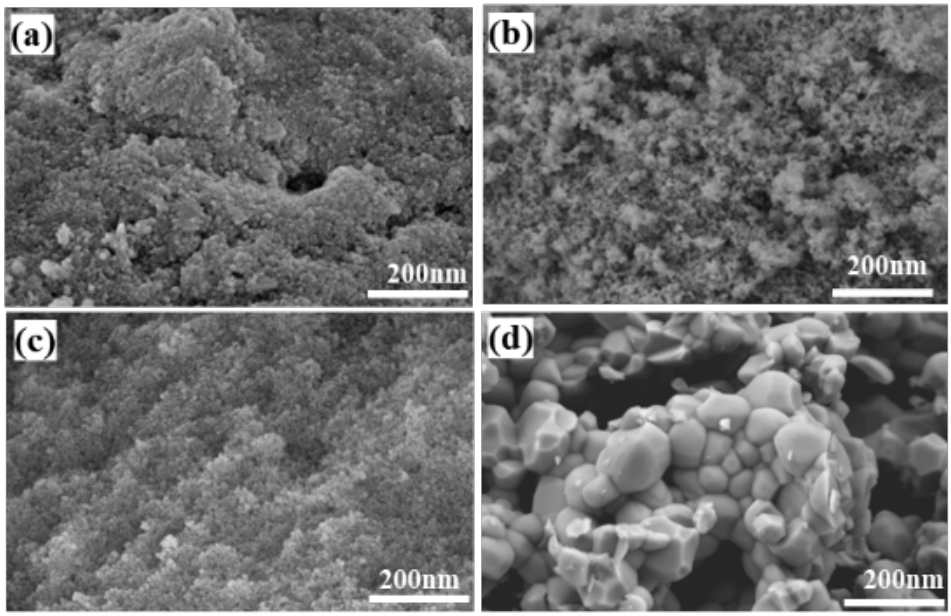

Fig.4 FESEM images: (a) $CuFe_2O_4$; (b) $NiFe_2O_4$; (c)$CoFe_2O_4$; (d) $(FeCoNiCrZnCu)_3O_4$

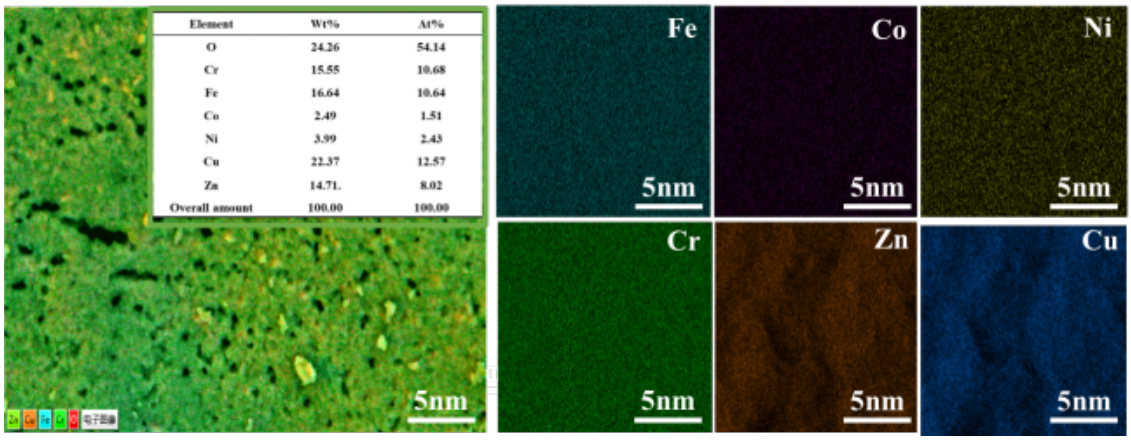

Fig.5 EDS mapping of $(FeCoNiCrZnCu)_3O_4$

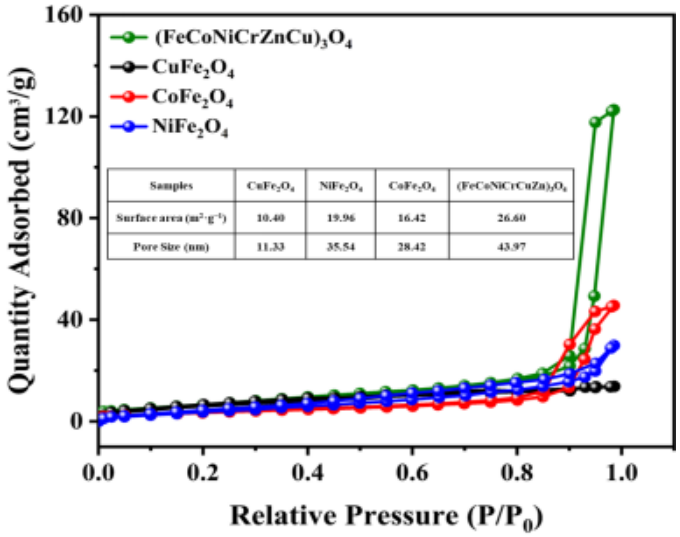

Fig.6 BET plots of $CuFe_2O_4$, $NiFe_2O_4$, $CoFe_2O_4$, $(FeCoNiCrZnCu)_3O_4$

The valence states of the elements on the material's surface were determined

through X-ray Photoelectron Spectroscopy (XPS) analysis, and the energy spectra of the elements Co, Fe, Cr, Zn, Ni, Cu and O are shown in **Fig.7**, corrected by the C1s peak (284.80 eV). For $(FeCoNiCrZnCu)_3O_4$, the two peaks at 710.66 and 723.84 eV were associated with the spin-orbit splitting peaks of Fe^{2+} $2p_{3/2}$ and Fe^{2+} $2p_{1/2}$, while the spin-orbit peaks of Fe^{3+} $2p_{1/2}$ and Fe^{3+} $2p_{3/2}$ are located at 726.05 eV and 712.83 , individually [25]. In this study, the potential energy positions of $(FeCoNiCrZnCu)_3O_4$, $CuFe_2O_4$, $NiFe_2O_4$, and $CoFe_2O_4$ exhibit varying degrees of shift. As shown in **Fig. 7a,** the Fe peak in $(FeCoNiCrZnCu)_3O_4$ is shifted to a higher binding energy, indicating a change in the electronic structure after the formation of the high entropy structure. A similar shift is also observed in the Cu 2p, Ni 2p, and Co 2p peaks, further confirming that the high entropy effect influences the electronic properties of the materials. This shift suggests the involvement of synergistic interactions between the metal cations, which may enhance the catalytic performance by modifying the electronic environment at the active sites. These observations consistently indicate that the reconstruction of electronic structure is a common phenomenon in the formation of high entropy [32]. Nevertheless, iron can inhibit the generation of unwanted oxides by ensuring charge stability, which could negatively impact the creation of reactive sites [33]. Fortunately, Fe^{3+} is able to activate Co^{3+} through charge and spin effects, thus effectively increasing the intrinsic activity of $(FeCoNiCrZnCu)_3O_4$ [34]. In the Co 2p energy spectrum, the peaks observed at 781.46 eV and 797.19 eV correspond to the spin-orbit splitting in the Co^{2+} $2p_{3/2}$ and Co^{2+} $2p_{1/2}$ energy levels. Conversely, the spin-orbit coupling peaks for Co^{3+} $2p_{3/2}$ and Co^{3+} $2p_{1/2}$ are identified at 780.08 eV and 795.50 eV, respectively [35]. The signals of Ni^{2+} (855.12 eV and 872.41 eV) and Ni^{3+} (856.70 eV and 874.34 eV) were attributed to the Ni $2p_{3/2}$ and Ni $2p_{1/2}$ orbitals, respectively [35]. The signals of Cr^{3+} (576.65 eV) and Cr^{6+} (579.39 eV) were associated with the Cr $2p_{3/2}$ orbital [25]. The $2p_{3/2}$ and $2p_{1/2}$ orbitals of Cu^{2+}/Zn^{2+} were located at 934.67/1021.31 and 954.14/1044.39 eV [36, 37]. Variations in ionic radii and valence states among Fe, Co, Ni, Cr, Zn, and Cu lead to lattice deformations, subsequently influencing the local electronic configuration and the ionic valency. Such lattice distortions may lead to the tuning of elemental valence states, which can have a significant effect on the catalytic

performance [38]. Zn and Cu cations all showed divalent, Fe, Co, and Ni cations were all in mixed valence states of +3 and +2, while Cr was in mixed valence states of +3 and +6. This valence distribution suggests that the introduction of low-valence cations facilitate the production of oxygen vacancies. [39], whereas the rise in high-valence metal cations aids in enhancing chemisorption and redox processes [15], which together markedly improve the catalytic activity of OER. During the formation of chemical bonds, electrons from high-valent transition metals (TMs) tend to accumulate on their surfaces. This electron enrichment phenomenon strengthens the covalent metal-oxygen (M-O) interactions and thus favours the promotion of OER [40]. Cu^{2+} doping to $(FeCoNiCrZnCu)_3O_4$ accelerates charge transfer [41], whereas the increased presence of Ni^{2+} offers pathways for carrier transport. [42].

In the O1s energy spectrum, the observed peaks at 529.66 eV, 531.67 eV, and 532.80 eV are attributed to lattice oxygen (O_1, representing metal-oxygen bonds M-O), oxygen defects (O_2, linked to oxygen vacancies O_V), and surface-adsorbed oxygen (O_3), respectively [43]. The calculation of the peak areas showed that the O_V contents of $(FeCoNiCrZnCu)_3O_4$, $CuFe_2O_4$, $NiFe_2O_4$, $CoFe_2O_4$, were 43.23, 19.95, 24.00 and 25.60 %, respectively, which indicated that the highest O_V concentrations were found in $(FeCoNiCrZnCu)_3O_4$. In this paper, we demonstrate the effect of oxygen vacancies on catalytic performance by EPR and XPS. Oxygen vacancies may effectively modulate the electronic density of states at metal sites and directly participate in the formation of O-O bonds through the lattice oxygen mechanism (LOM) [44]; meanwhile, their introduction may enhance the electron transport capacity [45]. A Higher content of oxygen vacancies favors the conductivity of the material, which in turn accelerates the charge transport. O_V regulate electron transport capacity, promote oxidation processes, and increase catalyst activity. Through the creation of additional active sites, they aid in the breakdown of water molecules and the liberation of oxygen [39].

In summary, the elements of Co, Fe, Ni and Cr may act together to promote OER, thus improving the overall catalyst performance in $(FeCoNiCrZnCu)_3O_4$, a composite oxide, while at the same time, the elements of Zn and Cu may play a role in promoting HER, which contributes to the efficiency of hydrogen generation. This rational design of

materials and synergistic effects between elements provide an efficient catalyst solution for electrocatalytic water decomposition.

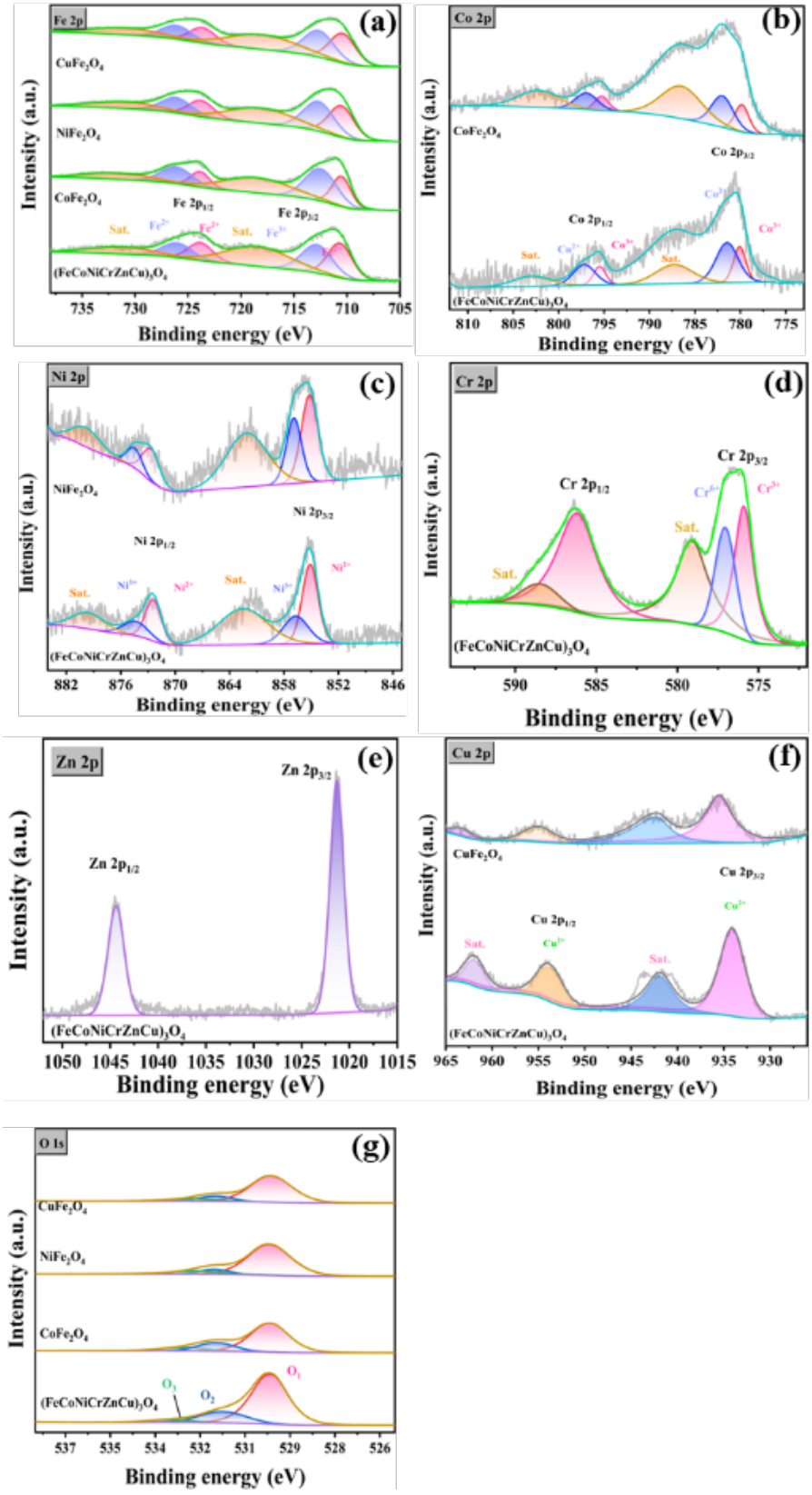

Fig.7 XPS images of $CuFe_2O_4$, $NiFe_2O_4$, $CoFe_2O_4$, $(FeCoNiCrZnCu)_3O_4$

Table 1 Statistics of different oxygen species of $CuFe_2O_4$, $NiFe_2O_4$, $CoFe_2O_4$, and $(FeCoNiCrZnCu)_3O_4$

Sample	O_1	O_2	O_3
$CuFe_2O_4$	78.14%	13.29%	8.56%
$NiFe_2O_4$	78.50%	8.76%	12.75%
$CoFe_2O_4$	69.88%	21.03%	9.09%
$(FeCoNiCrZnCu)_3O_4$	47.66%	48.01%	4.32%

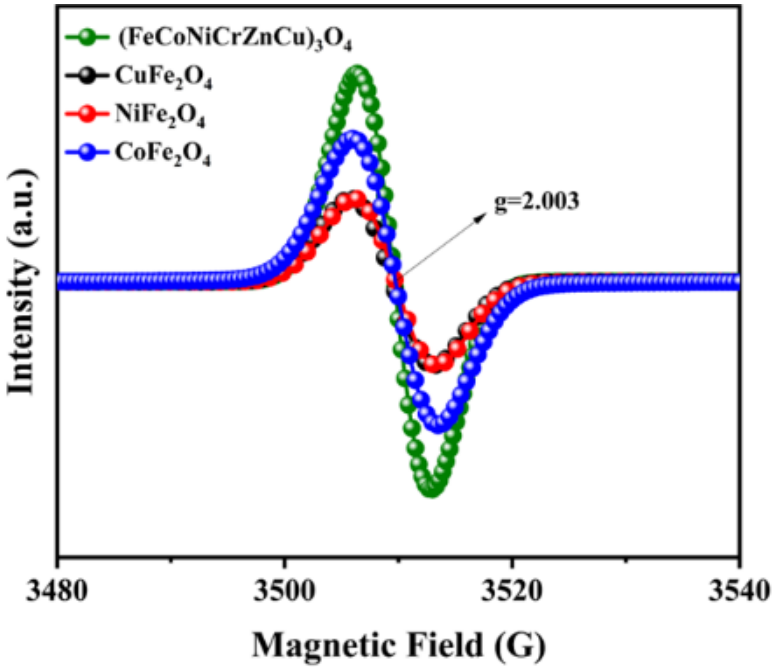

Fig.8 EPR plots of $CuFe_2O_4$, $NiFe_2O_4$, $CoFe_2O_4$, $(FeCoNiCrZnCu)_3O_4$

The HER properties of the oxides were evaluated using a standard three-electrode setup. As shown in **Figs. 9a and 9c**, the overpotential of $(FeCoNiCrZnCu)_3O_4$ at 10 mA cm^{-2} is 133 mV, which is significantly lower than that of $CuFe_2O_4$ (210 mV), $NiFe_2O_4$ (178 mV), and $CoFe_2O_4$ (195 mV). **Fig. 9b** presents the Tafel slopes for HER, where the Tafel slope of $(FeCoNiCrZnCu)_3O_4$ is 116 mV dec^{-1}), notably lower than the slopes of $CuFe_2O_4$ (144 mV dec^{-1}), $NiFe_2O_4$ (132 mV dec^{-1}), and $CoFe_2O_4$ (140 mV dec^{-1}). This indicates that $(FeCoNiCrZnCu)_3O_4$ exhibits the fastest reaction kinetics. The Tafel slope also supports the conclusion that the HER process at the electrode follows the Volmer-Heyrovsky mechanism, which involves the adsorption of hydrogen atoms

(Volmer step) and their subsequent combination (Heyrovsky step) to form H_2.

Similarly, the electrocatalytic performance for the OER of the catalysts was evaluated under alkaline conditions using a standard three-electrode system. Among the four catalyst, $(FeCoNiCrZnCu)_3O_4$ demonstrated the best catalytic activity. At a current density of 10 mA cm^{-2}, $(FeCoNiCrZnCu)_3O_4$ exhibited an overpotential of only 357 mV, significantly lower than that of $CuFe_2O_4$ (408 mV), $NiFe_2O_4$ (415 mV), and $CoFe_2O_4$ (390 mV) as show in **Figs.9e and 9g**. The results suggest that these elements, when combined in a high-entropy structure, effectively enhance the OER activity, making $(FeCoNiCrZnCu)_3O_4$ a promising candidate for improving electrocatalytic efficiency in water electrolysis applications. The Tafel slope provides insights into the kinetic behavior of the OER. As seen in the **Fig.9f,** the Tafel slope for $(FeCoNiCrZnCu)_3O_4$ is 116 mV dec^{-1}, which is significantly lower than that of $CuFe_2O_4$ (144 mV dec^{-1}), $NiFe_2O_4$ (132 mV dec^{-1}), and $CoFe_2O_4$ (140 mV dec^{-1}). This indicates that $(FeCoNiCrZnCu)_3O_4$ has faster reaction kinetics, further confirming its superior OER performance compared to the non-high entropy spinel catalysts. The lower Tafel slope suggests that the high entropy structure, with its rich and diverse elemental composition, effectively promotes the reaction kinetics of the OER process.

Usually, The effectiveness of a catalyst is intimately linked to the oxidation state of the surface-active centers [46]. It has been Reported that catalysts with higher metal oxidation state active centers on the surface will exhibit enhanced OER performance as they are more likely to accept electrons during the OER process [47]. The XPS analysis revealed that the altering composition of metal elements within $(FeCoNiCrZnCu)_3O_4$ resulted in distinct alterations to the oxidation states of the catalyst's constituents. The maximum proportions of Cr^{6+} and Co^{3+} were detected in the $(FeCoNiCrZnCu)_3O_4$ composition, and the positions of their orbital peaks were moved to greater binding energies, which implies that the OER activities of Cr and Co in $(FeCoNiCrZnCu)_3O_4$ are higher. In addition, $(FeCoNiCrZnCu)_3O_4$ boasts the greatest concentration of oxygen vacancies (O_V). Furthermore, the incorporation of O_V can enhance catalytic dynamics by refining the electronic configuration, boosting the carrier density, and offering extra unsaturated active sites [48]. As a result, $(FeCoNiCrZnCu)_3O_4$

demonstrates a significantly smaller Tafel slope compared to the other tested materials, with faster reaction kinetics, and the variation of this trend is not only related to the introduced metal elements (Cr, Zn, and Cu), but also due to the synergistic interaction among certain metals.

In addition, to ascertain the electrochemically active surface area (ECSA), the relationship between the scan rate and the current density was investigated, as shown in **Fig.9 d.** The Cdl of the four samples were 2.8 mF cm^{-2}, 1.23 mF cm^{-2}, 1.23 mF cm^{-2}, 1.9 mF cm^{-2}, respectively, suggesting that $(FeCoNiCrZnCu)_3O_4$ has a higher density of active sites, which is favourable for HER and OER reactions. This result also provides further evidence that the physical and chemical properties of oxides can be optimised by regulating the type of metal elements present in them. To assess the charge transfer capability of the material, electrochemical impedance spectroscopy (EIS) measurements were then performed. The fitted Nyqust plot is shown in **Fig.9 h**. The charge transfer resistance (Rct.) of each sample was in the order of $(FeCoNiCrZnCu)_3O_4$ (0.31 Ω) < $CuFe_2O_4$ (0.49 Ω) < $CoFe_2O_4$ (0.67 Ω) < $NiFe_2O_4$ (1.62 Ω). The FCNCCZ-O sample has the smallest transfer resistance, which allows for a fast transfer of charge and thus enhances the catalytic performance.

Furthermore, the $(FeCoNiCrZnCu)_3O_4$ preserved outstanding stability for a duration of 50 h (the HER decayed by 8% and the OER decayed by 5%.) when subjected to the concurrent current technique at a density of 100 mA cm^{-2} (**Fig.10**). This suggests that $(FeCoNiCrZnCu)_3O_4$ possesses superior cycle retention. This is strongly associated with a considerable rise in configurational entropy, stemming from the random distribution of various metal elements occupying identical sites. XRD results show that there is no obvious change in the characteristic peaks of the spinel structure in the XRD spectrum of $(FeCoNiCrZnCu)_3O_4$ before and after the stability test, confirming that the material maintains excellent crystal structure stability after long-term electrochemical testing (**Fig.2**), which is closely related to the mechanism of multiple components in the high entropy system synergistically inhibiting lattice remodeling [49]. SEM shows that the nanoparticles have slight agglomeration (**Fig.11**), which may be due to the reduction of surface energy caused by electrolyte infiltration,

but the EDS element distribution diagram (**Fig.11**) confirms that the six elements of Fe, Co, Ni, Cr, Zn, and Cu are evenly dispersed [50].

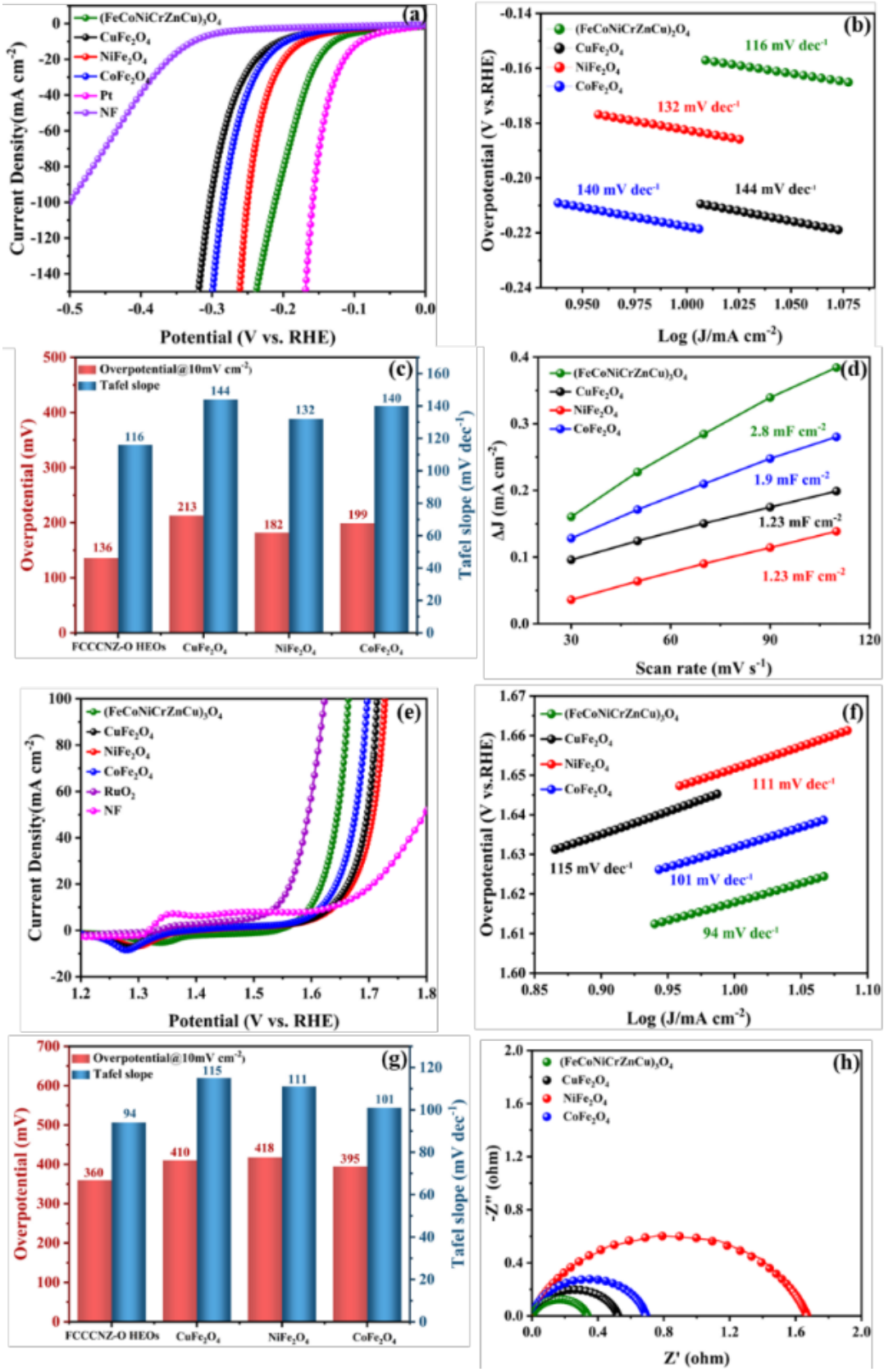

Fig.9 $CuFe_2O_4$, $NiFe_2O_4$, $CoFe_2O_4$, $(FeCoNiCrZnCu)_3O_4$

(a), (c) LSV; (b), (d) Tafel; (e) Cdl; (f) EIS

Table 2 Comparison of electrochemical performance of synthesized $(FeCoNiCrZnCu)_3O_4$ and catalysts reported in literature

Sample	OER Overpotential at 10 mA/cm^2 (mV)	HER Overpotential at 10 mA/cm^2 (mV)	Refs.
$(FeCoNiCrZnCu)_3O_4$	357	133	This work
$(FeCoNiCrMnCu)_3O_4$	241.4	-	[51]
$(Cr_{1/5}Mn_{1/5}Ni_{1/5}Fe_{1/5}Co_{1/5})_3O_4$	411	-	[52]
$(FeCoNiCrMn)_3O_4$	239	-	[53]
$(FeCoNiCrMg)_3O_4$	278	-	[15]
$(FeCoNiCrMn)_3O_4$	298	-	[15]
$(FeCoNiCrZn)_3O_4$	306	-	[15]
$(FeCoNiCrCu)_3O_4$	338	-	[15]
$(AlCrCoNiFe_2)_3O_4$	230	-	[14]
CoCrFeNiMo	273	-	[54]
FeCoNi-MoO	204	-	[55]
Co_3S_4	270	-	[17]
CoNiP	400	116	[56]
Ni(CoNi)O	349	-	[57]
Ni-Co_3O_4	380	-	[58]
Zn-Co_3O_4	420	-	[58]
$NiFe_2O_4$	450	-	[59]
$CoFe_2O_4$	410	-	[59]

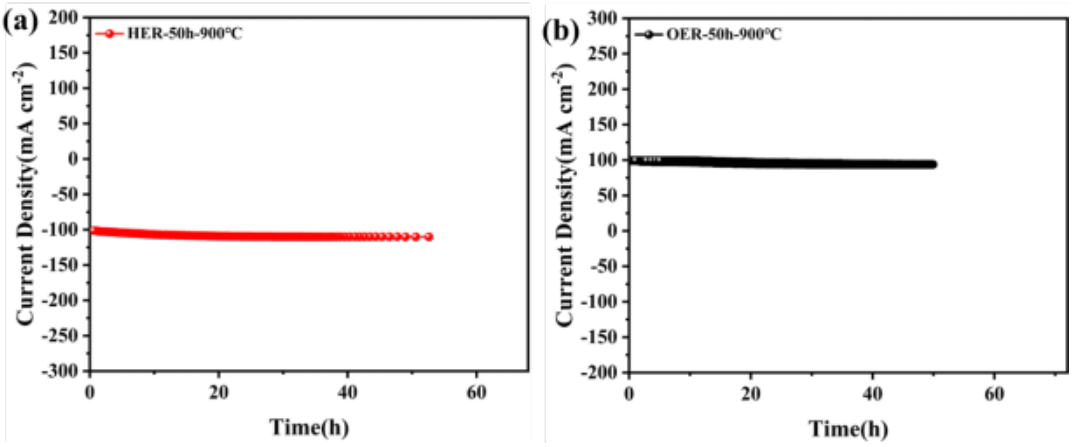

Fig. 10 Chrono-current test of $(FeCoNiCrZnCu)_3O_4$ at a density of 100 mA cm^{-2}

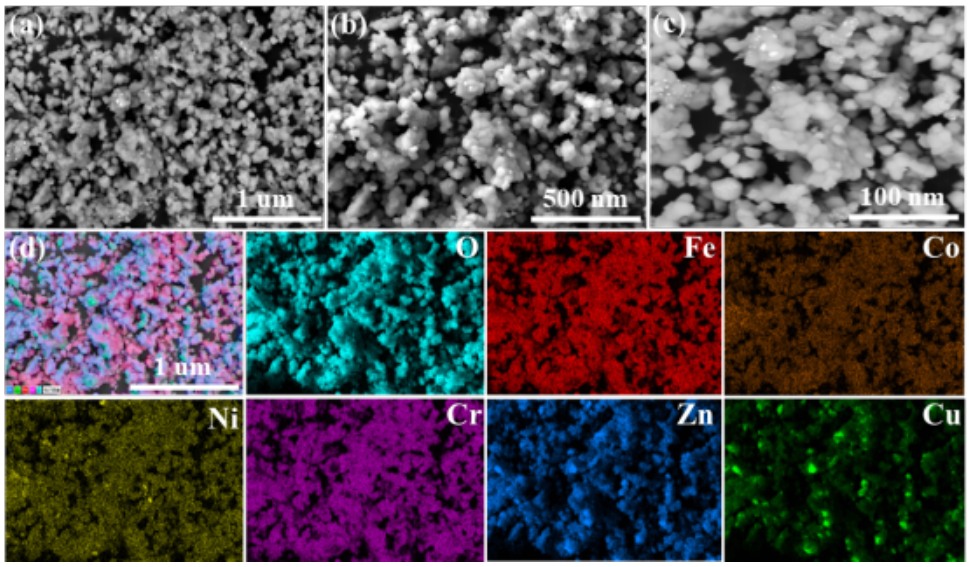

Fig. 11 SEM plot after stability test

4 Conclusion

In this work, a high-entropy spinel $(FeCoNiCrCuZn)_3O_4$ catalyst with bifunctional catalytic properties was successfully synthesized using the microwave hydrothermal method. Under alkaline conditions, the $(FeCoNiCrCuZn)_3O_4$ catalyst exhibited outstanding catalytic performance, achieving hydrogen evolution reaction (HER) and oxygen evolution reaction (OER) overpotentials of 133 mV and 357 mV, respectively, at a current density of 10 mA/cm^2. These values are lower than those of conventional non-high-entropy spinel materials such as $CuFe_2O_4$, $NiFe_2O_4$, and $CoFe_2O_4$, highlighting the superior catalytic efficiency of $(FeCoNiCrCuZn)_3O_4$. The remarkable catalytic activity of $(FeCoNiCrCuZn)_3O_4$ can be attributed to the high-entropy strategy, which enhances the formation of oxygen vacancies, as well as the presence of multiple metal cations with variable oxidation states. Furthermore, chromo-current testing over 50 hours revealed negligible current density decay, demonstrating the catalyst's interesting stability. This work underscores the potential of high-entropy spinel materials for water electrolysis applications and provides a valuable reference for designing cost-effective electrocatalysts.

CRediT authorship contribution statement

Mingxu LI: methodology, formal analysis, investigation, data curation and writing - original draft. Xiaolei YE: formal analysis and writing - review & editing. Shenghui

GUO: formal analysis. Ming HOU: funding acquisition, supervision and writing - review & editing. Li YANG: formal analysis. Kaihua CHEN: funding acquisition, conceptualization. Lei GAO: formal analysis and software. Pascal BRIOIS: formal analysis. Yunchuan LI: conceptualization, funding acquisition, supervision and writing - review & editing. Pascal BRIOIS：language review, formal analysis and visualization.

Acknowledgement

This research was supported by National Natural Science Foundation of China (52364051, 52374389) and Caiyun Postdoctoral Program in Yunnan Province of China (CG24056E003A, CG24056E014A).

Reference

[1] Grasso M, Delatin Rodrigues D. Rage against the fossil machine: The deactivation of fossil energy production in Italy. ENERGY RES SOC SCI. 2024;115:103655.

[2] Wu Q, Chen M, Ren H, Li Q, Gao W. Collaborative modeling and optimization of energy hubs and multi-energy network considering hydrogen energy. RENEW ENERG. 2024;227:120489.

[3] Zeng G, Liu M, Lei Z, Zhang S, Chen Z. Optimal configuration of hydrogen energy storage in an integrated energy system considering variable hydrogen production efficiency. J ENERGY STORAGE. 2024;98:113044.

[4] Zakaria Z, Kamarudin K, Ikhmal N, Rosyadah N, Aminuddin A, Hanapi H, et al. Energy scenario in malaysia: Embarking on the potential use of hydrogen energy. INT J HYDROGEN ENERG. 2023;48:35685-707.

[5] Akhtaruzzaman M, Rahman R. Commonality in systemic risk from green and conventional energy. ENERG ECON. 2024:107404.

[6] Hachem C, Singh K. Energy systems and energy sharing in traditional and sustainable archetypes of urban developments. SUSTAINABILITYBASEL. 2022; 14(3):1356.

[7] Yang R, Wang F, Rao Z, Shen C, Li D. Advancing sustainable energy solutions: innovations in clean energy applications and conventional energy efficiency upgrade. ENERGIES. 2024; 17(10), 2441.

[8] Xu L, Yang J. Carbon pricing policies and renewable energy development: Analysis

based on cross-country panel data. J ENVIRON MANAGE. 2024;366:121784.

[9] Segawa Y, Endo N, Shimoda E, Yamane T, Maeda T. Pilot-scale hydrogen energy utilization system demonstration: A case study of a commercial building with supply and utilization of off-site green hydrogen. INT J HYDROGEN ENERG. 2024;50:26-36.

[10] Ham K, Bae S, Lee J. Classification and technical target of water electrolysis for hydrogen production. J ENERGY CHEM. 2024;95:554-76.

[11] Xu Y, Qu G, Wu H, Zhao C, Xu R, Ning P, et al. Synthesis and optimization of foam copper-based CoMnOx@Co_3O_4/CF catalyst: Achieving efficient catalytic oxidation of paraxylene. ACS Appl Mater Interfaces. 2024;16(45):61970-61982.

[12] Jiang Y, Liang Z, Fu H, Sun M, Wang S, Huang B, et al. Pt-modified high entropy rare earth oxide for efficient hydrogen evolution in pH-universal environments. J Am Chem Soc. 2024;146:9012-25.

[13] Liu X, Guo X, Gong M, Deng S, Liang J, Zhao T, et al. Corrosion-assisted large-scale production of hierarchical iron rusts/$Ni(OH)_2$ nanosheet-on-microsphere arrays for efficient electrocatalysis. ELECTROCHIM ACTA. 2020;353:136478.

[14] Dadvari P, Hung W, Wang K. High entropy spinel oxide $(AlCrCoNiFe_2)O$ as highly active oxygen evolution reaction catalysts. ACS Omega. 2024;9:27692-8.

[15] Guo Y, Zhang X, Wei H, Yu H-t, Xie Y. Construction of spinel $(Fe_{0.2}Co_{0.2}Ni_{0.2}Cr_{0.2}M_{0.2})_3O_4$ (M = Mg, Mn, Zn, and Cu) high-entropy oxides with tunable valance states for oxygen evolution reaction. J ALLOY COMPD. 2024;989:174304.

[16] Liu Y, Ding M, Deng X, Zhang Y, Zhao G. Bimetal phosphide as high efficiency and stable bifunctional electrocatalysts for hydrogen and oxygen evolution reaction in alkaline solution. RSC ADV. 2022;12:9051-7.

[17] Li X, Zheng K, Zhang J, Li G, Xu C. Engineering sulfur vacancies in spinel-phase Co_3S_4 for effective electrocatalysis of the oxygen evolution reaction. ACS Omega. 2022;7:12430-41.

[18] Zeng R, Li H, Shi Z, Xu L, Meng J, Xu W, et al. Origins of enhanced oxygen reduction activity of transition metal nitrides. NAT MATER. 2024; 23:1695-1703.

[19] Zhang S, Cheng Y, Wang P, Lei X, You J, Guo R, et al. Research progress on surface reconstruction of transition metal sulfides (TMS, M=Fe, Co, Ni) as precatalysts for oxygen evolution reaction. INT J HYDROGEN ENERG. 2024;51:545-60.

[20] Wang Y, Wang L, Fu H. Research progress of Fe-N-C catalysts for the electrocatalytic oxygen reduction reaction. SCI CHINA MATER. 2022;65:1701-22.

[21] Jin S. Are metal chalcogenides, nitrides, and phosphides oxygen evolution catalysts or bifunctional catalysts? ACS Energy Lett. 2017;2:1937-8.

[22] Rost M, Sachet E, Borman T, Moballegh A, Dickey E, Hou D, et al. Entropy-stabilized oxides. NAT COMMUN. 2015;6:8485.

[23] Nguyen X, Patra J, Chang K, Ting M. High entropy spinel oxide nanoparticles for superior lithiation-delithiation performance. J MATER CHEM A. 2020;8:18963-73.

[24] Sun Z, Zhao Y, Sun C, Ni Q, Wang C, Jin H. High entropy spinel-structure oxide for electrochemical application. CHEM ENG J. 2022;431:133448.

[25] He L, Kang H, Hou G, Qiao X, Jia X, Qin W, et al. Low-temperature synthesis of nano-porous high entropy spinel oxides with high grain boundary density for oxygen evolution reaction. CHEM ENG J. 2023;460:141675.

[26] Wang W, Liu B, He C, Zhao P, Zhao S, Wang Z, et al. High-entropy engineering for broadband infrared radiation. ADV FUNCT MATER. 2023;33:2303197.

[27] Amarnath P, Madhu R, Praveen K, Govindarajan S, Kundu S, Subramaniam Y. Phase-pure high-entropy spinel oxide $(Ni,Fe,Mn,Cu,Zn)_3O_4$ via thermal plasma: A promising electrocatalyst for oxygen evolution reaction. ACS Appl. Energy Mater. 2023;6:5899-911.

[28] Du C, Xue Y, Liang H, Wang C, Zeng Q, Wang J, et al. Exploring the oxidation behaviors of the TiVCrMo high-entropy MAX at 800 °C for its self-lubricity. J MATER SCI TECHNOL. 2024;187:49-62.

[29] Wang D, Liu Z, Du S, Zhang Y, Li H, Xiao Z, et al. Low-temperature synthesis of small-sized high-entropy oxides for water oxidation. J MATER CHEM A. 2019;7:24211-6.

[30] Ouyang X, Zhang Z, Qin T, Pei Z, Guo X. Macroporous high-entropy spinel oxide monoliths as efficient oxygen evolution electrocatalyst. J AM CERAM SOC.

2024;107:8354-66.

[31] Talluri B, Yoo K, Kim J. High entropy spinel metal oxide $(CoCrFeMnNi)_3O_4$ nanoparticles as novel efficient electrocatalyst for methanol oxidation and oxygen evolution reactions. J ENVIRON CHEM ENG. 2022;10:106932.

[32] Sun N, Zheng Z, Lai Z, Wang J, Du P, Ying T, et al. Augmented electrochemical oxygen evolution by d-p orbital electron coupling. ADV MATER. 2024;36:2404772.

[33] Kim B, Fabbri E, Abbott D, Cheng X, Clark A, Nachtegaal M, et al. Functional role of Fe-doping in Co-based perovskite oxide catalysts for oxygen evolution reaction. J Am Chem Soc. 2019;141:5231-40.

[34] Wang X, Ouyang T, Wang L, Zhong J, Ma T, Liu Z. Redox-inert Fe^{3+} ions in octahedral sites of Co-Fe spinel oxides with Enhanced oxygen catalytic activity for rechargeable zinc-air batteries. ANGEW CHEM INT EDIT. 2019;58:13291-6.

[35] Chen J, Wang K, Liu Z, Sun X, Zhang X, Lei F, et al. Sulfurization-induced lattice disordering in high-entropy catalyst for promoted bifunctional electro-oxidation behavior. CHEM ENG J. 2024;489:151234.

[36] Xu L, Wang L, Li Y, Song Q, Tian Z, Wang C, et al. A novel high-entropy spinel ferrites $(CoNiCuZnMg)Fe_2O_4$ catalyst for H_2 production via steam reforming of derived volatiles from polypropylene and waste cooking oil. CHEM ENG J. 2024;488:150767.

[37] Chen X, Zhang N, Wang H, Zhong Y, Lv T, Liang C. $PtPdCoNiCu/TiO_2$ High-Entropy alloy catalyst for synthesis of γ-Butyrolactone by selective hydrogenation of maleic anhydride. CHEM ENG J. 2024;490:151672.

[38] Li H, Lai J, Li Z, Wang L. Multi-sites electrocatalysis in high-entropy alloys. ADV FUNCT MATER. 2021;43: 4639-4776.

[39] Zhu K, Shi F, Zhu X, Yang W. The roles of oxygen vacancies in electrocatalytic oxygen evolution reaction. NANO ENERGY. 2020;73:104761.

[40] Liu F, Yu M, Chen X, Li J, Liu H, Cheng F. Defective high-entropy rocksalt oxide with enhanced metal-oxygen covalency for electrocatalytic oxygen evolution. CHINESE J CATAL. 2022;43:122-9.

[41] Li W, Gao X, Wang X, Xiong D, Huang P, Song W, et al. From water reduction to oxidation: Janus Co-Ni-P nanowires as high-efficiency and ultrastable electrocatalysts

for over 3000h water splitting. J POWER SOURCES. 2016;330:156-166.

[42] Li S, Liu T, Zhang W, Wang M, Zhang H, Qin C, et al. Highly efficient anion exchange membrane water electrolyzers via chromium-doped amorphous electrocatalysts. NAT COMMUN. 2024;15:3416.

[43] Lao Y, Huang X, Liu L, Mo X, Huang J, Qin Y, et al. Structure-activity relationship study of high entropy oxides catalysts for oxygen evolution reaction. CHEM ENG J. 2024;481:148428.

[44] Fu L, Zhou S, Xiang M, Yang J, Fan W, Yang Z, et al. Advances in anion vacancy for electrocatalytic oxygen evolution reaction. J ELECTROANAL CHEM. 2022;921:116650.

[45] Zhang L, Xie X, Wang H, Ji L, Zhang Y, Chen H, et al. Boosting electrocatalytic N_2 reduction by MnO_2 with oxygen vacancies. CHEM COMMUN. 2019;55:4627-4630.

[46] Ward TR, Copéret C. Introduction: bridging the gaps: learning from catalysis across boundaries. Chem Rev. 2023;123:5221-5224.

[47] Mu X, Yu M, Liu X, Liao Y, Chen F, Pan H, et al. High-entropy ultrathin amorphous metal-organic framework-stabilized Ru(Mo) dual-atom sites for water oxidation. ACS Energy Lett. 2024:5763-5770.

[48] Zhang H, Wu L, Feng R, Wang S, Hsu C, Ni Y, et al. Oxygen vacancies unfold the catalytic potential of NiFe-layered double hydroxides by promoting their electronic transport for oxygen evolution reaction. ACS Catal. 2023;13:6000-6012.

[49] Li J, Chen Y, He Q, Xu X, Wang H, Jiang C, et al. Heterogeneous lattice strain strengthening in severely distorted crystalline solids. P NATL A SCI INDIA B. 2022;119(25):e2200607119.

[50] Ahirwar B, Kumar A. Experimental investigation for heat transfer performance of CuO-water nanofluid in a double pipe heat exchanger. J THERM ANAL CALORIM. 2024;149:4133-4151.

[51] Wang J, Zhang J, Yu H, Chen L, Jiang H, Li C. Strain engineering of high-entropy oxides enriches highly active lattice oxygen for electrocatalytic water oxidation. ACS Materials Lett. 2024;6:1739-1745.

[52] Du Y, Yang F, Li J, Jiang M, Yin J, Hu Q, et al. Electrocatalytic performances of

high-entropy spinel oxide $(Cr_{1/5}Mn_{1/5}Ni_{1/5}Fe_{1/5}Co_{1/5})_3O_4$ for oxygen reduction/evolution reactions in alkaline electrolyte. J ALLOY COMPD. 2024;1004:175923.

[53] Feng B, Chen J, Yang Y, Yang M, Wang H, Zhong C, et al. Facile synthesis of nanosized spinel high entropy oxide $(FeCoNiCrMn)_3O_4$ for efficient oxygen evolution reaction. J MATERIOMICS. 2024;10:919-927.

[54] Huo X, Nie S, Zhang Y, Zuo X, Xu X, Zhang N, et al. Porous high-entropy alloy coatings as highly efficient electrocatalysts for electrocatalytic water splitting. CHEM ENG J. 2024;487:150622.

[55] Fan W, Liu C, Wang H, Wu J, Chen S, Fang W, et al. FeCoNi molybdenum-based oxides for efficient electrocatalytic oxygen evolution reaction. J COLLOID INTERF SCI. 2024;662:460-470.

[56] Liu Y, Ding M, Deng X, Zhang Y, Zhao G. Bimetal phosphide as high efficiency and stable bifunctional electrocatalysts for hydrogen and oxygen evolution reaction in alkaline solution. RSC ADV. 2022;12:9051-9057.

[57] Wang F, Chang S, Zhao Y, Yang H, Zhang Y. Fabricating highly-active Ni^{3+} sites of spinel to enhance electrocatalysis oxygen evolution reaction. INT J HYDROGEN ENERG. 2024;71:8-13.

[58] Vazhayil A, Ashok C, Thomas N. Probing the electrocatalytic activity of hierarchically mesoporous M-Co_3O_4 (M=Ni, Zn, and Mn) with branched pattern for oxygen evolution reaction. J ELECTROANAL CHEM. 2023;934:117298.

[59] Sultan F, González E, Medina I, Videa M, Sánchez M, Cholula-Díaz JL. Synthesis of MFe_2O_4 (M=Ni, Co) nanoparticles by a bicontinuous microemulsion method for the oxygen evolution reaction. ChemNanoMat. 2024;10: e202300541.